JSEE Vol. 26, No. 4, 2024 DOI: 10.48303/jsee.2024.2031074.1096

Research Paper

Investigating the Performance of Multi-Span Structures with Different Geometries and Heights under Near-Fault and Far-Fault Accelerations

Fahimeh Taghi Panahi[1] and Abbas Ali Akbarzadeh Morshedi[2*]

1. Assistant Professor, Department of Civil Engineering, Pooyesh Institute of Higher Education, Qom, Iran
2. Assistant Professor, Department of Civil Engineering, Kashan Branch, Islamic Azad University, Kashan/Isfahan, Iran,
*Corresponding Author; email: A.akbarzadeh@iaukashan.ac.ir

Received: 03/06/2024
Revised: 17/07/2024
Accepted: 17/08/2024

Keywords:
Dimensions;
Time-history analysis;
Masonry structure;
Seismic behavior

ABSTRACT

This work was a seismic assessment of arched masonry structures through a detailed analysis of three existing multi-span structures. Three structures with 1.27, 2.25 and 3.3 vault-to-spring ratios (L/B) with three different heights selected. The structures subjected to six near-fault and far-fault accelerations. When the number of spans increases, the stiffness and strength increases two times in the structure with a square plan and three times in the rectangular plan. Also from one span to two about 75% and from two to three about 30% increase in ductility is observed. In the multi-span structure of the narrower plan type, with the possible movement of the spans together, longitudinal failures also occur between the vaults. Increasing the height does not have much effect on the location of hinges, but it has a significant effect on increasing displacement. In the narrower structure, with the increase in height, the difference in the displacement of the spring to the vault has increased significantly and has been reported up to five times. In a square structure, this increase of the displacement is more than 50% and in narrower structures is about three times.

How to cite the article:
Taghi Panahi, F. and Akbarzadeh Morshedi, A. A. (2024). Investigating the Performance of Multi-Span Structures with Different Geometries and Heights under Near-Fault and Far-Fault Accelerations. *Journal of Seismology and Earthquake Engineering*, *26*(4), 53-69. doi: 10.48303/jsee.2024.2031074.1096

1. Introduction

The structural system of historical structures in Iran consists of ribbed vaults that allow gravity loads to be concentrated on four columns. Seismic evaluation of existing arched structures is necessary. The best method of seismic assessment is the limit analysis that accurately describes the seismic behavior of the masonry arch structure (Stockdale et al., 2018; Zampieri et al., 2019). Geometric damage and fatigue in masonry arches reduce the performance of the structure. Their analysis is needed to evaluate the capacity of structures to bear external loads (Zampieri et al., 2016).

Analyzing the effects of an earthquake on a historical structure is very important for cultural heritage organizations. To preserve and maintain them, it is essential to analyze the damage process, and appropriate numerical modeling methods should be developed to assess their vulnerability (Bartoli & Betti, 2013; Castori et al., 2017).

Types of research have been carried out on historical masonry structures experimentally and numerically, and there are many examples, including; historical arched masonry bridges (Gönen & Soyöz, 2021; Milani & Lourenço, 2012; Özmen & Sayin, 2018), towers (Castellazzi et al., 2018; Micelli & Cascardi, 2020), minarets and mosques (Altunis Sik & Genç, 2017; Gunes et al., 2021; Seker et al., 2014), churches (Atmaca et al., 2020; Hemeda, 2019; Kujawa et al., 2020) and chimneys (Masciotta et al., 2017). Specific structures, such as castles, fortresses, and fortifications, have been investigated regarding structural behavior (Tiberti et al., 2016).

It is necessary to understand the impact of near-fault and far-fault earthquakes on the stability of various structures. The effect of near-fault ground motions has been expressed more strongly (Talebi Jouneghani et al., 2017), and the researchers investigated the factors affecting the non-linear behavior of structures in the near-fault accelerations. The results showed that these earthquakes have behavior factors equal to or greater than design earthquakes on structures (Hatzigeorgiou, 2010). In this regard, researchers have stated that near-fault ground motions have more impact effects on structures than far-fault ground motions (Grimaz & Malisan, 2014). Also, the difference between near-fault and far-fault earthquakes on structures has investigated, which showed that the effects of far-fault earthquakes can be as crucial as near-fault earthquakes (Özmen & Sayin, 2021).

The current research is based on the article published in the 9th International Conference on Earthquake Identification and Earthquake Engineering (Taghi Panahi et al., 2024). This research examines the performance of multi-span historical vaulted masonry structures in different geometries and heights. Since these structures are historical monuments, it is necessary to know their performance ?under the acceleration of the earth. Also, examining the process of spreading damage and vulnerable areas in structures can provide better solutions for their maintenance and strengthening. In the present study, nonlinear dynamic time history analysis has been used to achieve unique and effective results. This analysis done using six records of the near-fault and far-fault earthquakes.

The structures were exposed to these accelerations from two directions. The displacement of the structure in the direction of acceleration and orthogonal direction, the acceleration of the ground input to the structure (a_g), and the plastic strain investigated in each analysis. It is worth mentioning that understanding the performance of structures in different plans and heights can open a new window in the maintenance or even reconstruction of such structures.

2. Structural Characteristics and Ground Motions of Case Studies

2.1. Near-Fault and Far-Fault Ground Motions

Pulse-type characteristics are essential properties of near-fault and far-fault ground motions; thus, six acceleration records selected. The acceleration and amplitude in Figure (1) and the information shown in Table (1).

One of the most critical points in time history analysis is the selection of accelerometers. To select the most appropriate acceleration, FEMA695 used, and the duration, magnitude, and number of accelerations selected according to its guidelines (Federal emergency management agency, 2009). The distance between near-fault and far-fault movements stated in various articles (Bayraktar & Hökelekli, 2020; Khan et al., 2019), which state that the near-fault earthquakes (<10 km) and the far-fault

earthquakes (20 to 100 km) are significantly different (Bayraktar & Hökelekli, 2020; Bertolesi et al., 2018; Güllü & Karabekmez, 2017; Szolomicki et al., 2015). The near-fault earthquake involves strong ground motion with a larger velocity pulse that inserts high energy into the structure, potentially increasing structural responses and causing significant damage (Cao & Ronagh, 2014; Davoodi

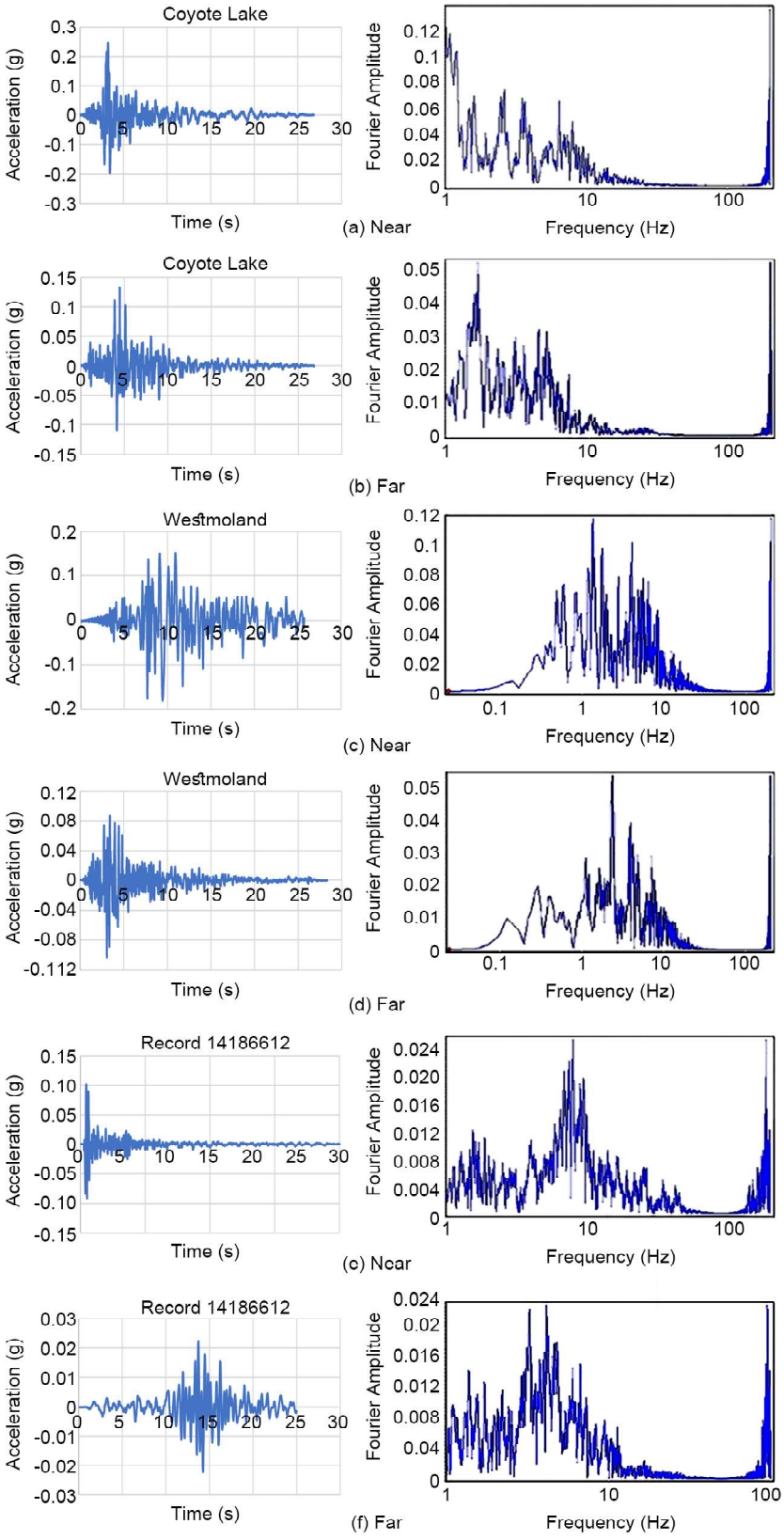

Figure 1. Selected acceleration and Fourier amplitudes: (a and b) near-fault and far-fault Coyote Lake; (c and d) near-fault and far-fault Westmorland; (e and f) near-fault and far-fault record 14186612.

Table 1. Properties of selected near-fault and far-fault accelerations.

Name	Earthquake Name	V_s (m/s)	PGA(g)	M_w	Distance to Fault (KM)	T_s(s)
E1	Coyote Lake	349.85	0.25	5.74	7.42	6.2
E2	Coyote Lake	367.43	0.132	5.74	20.67	6.2
E3	Westmorland	191.14	0.18	5.9	7.57	8
E4	Westmorland	362.38	0.1	5.9	20.37	10
E5	14186612	289.87	0.1	4.69	3.15	5.52
E6	14186612	348	0.022	4.69	22.05	10

et al., 2013; Güllü & Karabekmez, 2017). There are different methods for selecting accelerations, and two methods used in this article. The first method based on the distance (M), the distance to the fault (R), the type of fault (F), the type of local soil (S) and the main cycle time of the structure ($S_a(T_1)$). The second method is using uniform line spectrum (UHS).

According to FEMA 695, two accelerations are needed in the time history analysis in the far and near fault.

If more accelerations are used, they should have seismic acceleration peaks close to each other, and the rest of the accelerations can have different seismic acceleration peaks (Federal emergency management agency, 2009).

2.2. Selection of Dimensions of Historical Structures

The investigated structures were two in Iran from the historical and scenic center of Kashan. Structures 1 and 3 are Tabatabaei House, built in the second half of the 13th century *AH* (19th century *CE*) during the Qajar dynasty. The other structure is part of the Aqha Bozorg Mosque in Kashan, also built in the 13th century *AH* (19th century *CE*) during the Qajar dynasty. The structures examined in three plans and at different heights. The height of the bases in all structures changed to 1800, 2800 and 3800 mm to evaluate their effect. The structure with various plans and their geometry can see in Figure (2).

3. Numerical (FE) Model Generation and Properties

3.1. Material Properties

A sensitive issue in all studies on the behavior of historical structures is the characterization of the mechanical properties of the materials (Llopis-Pulido et al., 2019). It is not possible to take material samples because of the limitations placed on the preservation of a monument. Therefore, in this research, the properties of materials have been used from previously published articles. These was done by considering materials similar to those in previously published articles (Valente & Milani, 2019) using the mechanical properties shown in Table (2).

Table 2. Mechanical properties for a numerical model of structures (Valente & Milani, 2019).

Material	Young's Modulus M_{pa}	Poisson's Ratio	Density (Kg/m^3)	Compression Strength M_{pa}	Tension Strength M_{pa}
	1500	0.2	1800	2.4	0.15

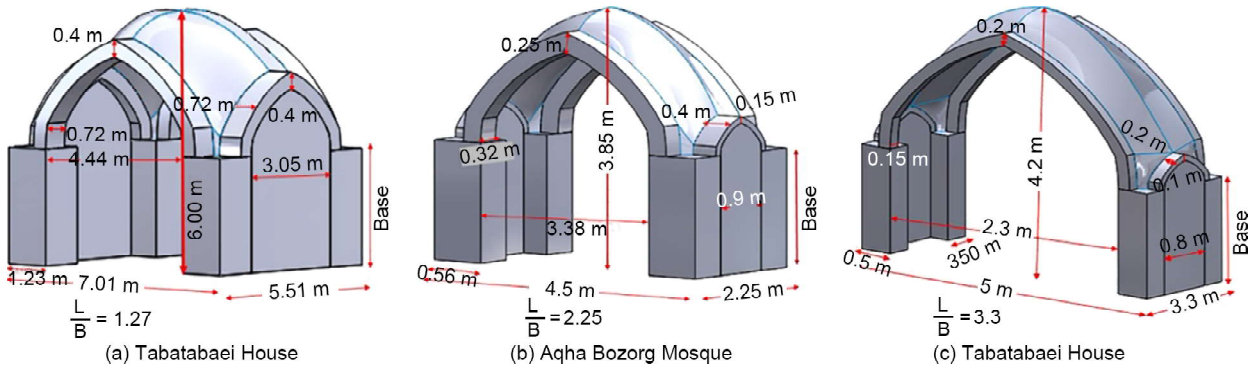

Figure 2. The dimensions of the structures with different plans and the height of the bases as variable elements in height.

3.2. Damage Plasticity Constitutive Model

A scalar variable was used to model failure under compression and tension in the damage plasticity constitutive model. This constitutive model simulates the effects of irreversible damage associated with failure mechanisms occurring in concrete and other quasi-brittle materials under low confining pressures. Concrete damage plasticity (CDP) model is useful for evaluating seismic-induced damage in structures. CDP is based on the mechanism of failure, i.e., tensile cracking and compressive crushing, of the analyzed structure (Zampieri et al., 2015) (Figure 3).

For all the materials involved in the analysis, a non-linear model is adopted. The main features of the model are the following: (1) linear and isotropic behavior in the elastic area and (2) elastic-plastic damageable behavior in the non-linear area, taking into account the difference between compressive and tensile strengths and the softening brittle behavior is reached. The plasticity-based damage model assumes that the main two failure mechanisms are tensile cracking and compressive crushing (Zhao et al., 2023). The parameters of the concrete damage model can see in Table (3).

The compressive stiffness was recovered after crack closure using loading variables from tension to compression. The tensile strength did not recover because of the changes in loading from compression to tension after creating micro-cracks. Under uniaxial stress conditions, the loss of elastic stiffness can be calculated as follows (Milani & Valente, 2015):

$$(1-d)=(1-S_t\,d_t)(1-S_c\,d_c) \tag{1}$$

where S_t and S_c are functions of the stress state and have been introduced to model the stiffness of recovery effects due to stress reversal. They can be computed using the following equations:

$$\begin{cases} S_t = 1-w_t(\sigma) & 0\le w_t\le 1 \\ S_c = 1-w_c\left(1-H(\sigma)\right) & 0\le w_c\le 1 \end{cases} \tag{2}$$

where w_t and w_c are the weight factors that control

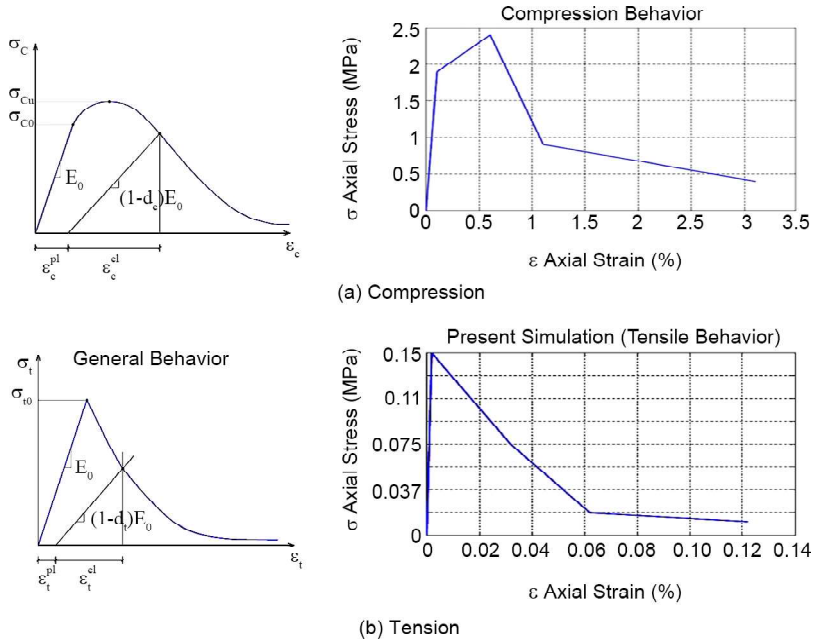

Figure 3. General non-linear uniaxial stress-strain behavior and for the present simulation under (Milani & Valente, 2015).

Table 3. Surface-to-surface contact parameters for interfaces (Bayraktar & Hökelekli, 2020).

			Surface-to-Surface Contact		
Interface	Normal behavior	Tangential behavior	Cohesive behavior		
Between Masonry	Hard	Friction Coefficient	Normal Stiffness (MPa/mm)	Shear Stiffness (MPa/mm)	
			K_{nn}	K_{ss}	K_{tt}
		0.3	0.36	0.175	0.175

recovery of the tensile and compressive stiffness, respectively, upon load reversal and show the uniaxial load cycle assuming the default behavior available in Abaqus, which correspond to $w_t = 0$ and $w_c = 1$ (D'Altri et al., 2019; Milani & Valente, 2015).

The simulations were performed by using the Abaqus code. The response under the damage plasticity constitutive model is affected by the following main parameters: dilation angle ψ, eccentricity ε; ratio f_{c0} / f_{bo} between the biaxial compressive yield strength and the uniaxial compressive yield strength; coefficient k; viscosity parameter χ, and the damage variables d_t and d_c (Abdulla et al., 2017; D'Altri et al., 2019) (Table 4).

Table 4. Constitutive parameter values for damage plasticity model for masonry (Milani & Valente, 2015).

Parameter	φ	ε	f_{co}/f_{bo}	k	χ
Amount	0.1	10	1.16	0.666	0.02

3.3. Interface Interaction Model

Interface elements were used to account for the plastic behavior and possible failure modes of the mortar. This done using the cohesive element in Abaqus. The shear and normal stress damage models also were used to allow for the degradation and removal of elements after failure. After mortar failure, the interaction between the blocks controlled by Mohr-Coulomb friction behavior (Nasiri & Liu, 2017). Contact assumed to be zero thickness; therefore, hard contact assigned as the normal behavior of general contact. These means that no penetration of the surfaces could occur (Bayraktar & Hökelekli, 2020) (Table 3).

Evaluation of the damping mechanisms in masonry structures is complex and has not yet been thoroughly investigated. In this study, the Rayleigh damping model considered, and the mass-proportional damping (a_0) and stiffness-proportional damping (a_1) coefficients assumed to be 0.35 and 0.00305, respectively. The New mark-beta method used for integration in the time domain (Zampieri et al., 2015).

3.4. Finite Element Modeling and Analysis

The 3D FE models of the studied buildings created using Abaqus software. SolidWorks software used to design the structures. The springs and vaults modeled integrally with the roof, and they didn't have the ability to move together. The bases and infill wall were modeled separately, and connected, then attached to the roof. The elements have the ability to slide and move and can slide together under the incoming forces.

The connection of the rib cover (roof, vault and spring), base and wall elements was made by spring modeling.

In this way, the normal and shear stiffness were defined and assigned to the joints. Columbus model used for friction modeling. To investigate the effect of height on structures, all analyses done with three different base heights of 1800, 2800 and 3800 mm separately. The behavior of masonry structures modeled with the concrete damage model, which explained in section 3.2.

To achieve better response convergence, mesh sensitivity analysis performed on three one-span structures. The results showed that the best mesh size, which has less effect on the maximum displacement and also saves analysis time, is 120 mm. Figure (4).

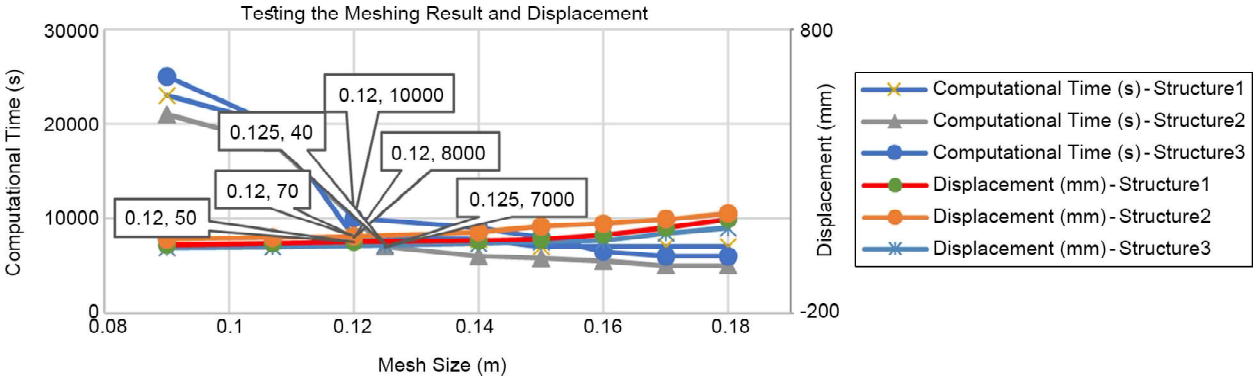

Figure 4. Mesh sensitivity analysis according to the applied force and maximum displacement.

For verification by the same authors, the 1:1 scale of structure examined in the laboratory in the past, and numerical analysis now done to verify the results. The test set-up can be seen in full in the article (Taghi Panahi et al., 2020), and these structures are taken from the historical structures of Iran. The materials of the model and the experimental structure are exactly the same as the structure under investigation.

In Figure (5), the longitudinal cracks in the roof, as well as the hinges at the spring and 1.4 vaults, are comparable. Shear-sliding cracks in foundations can confirm the accuracy of the modeling results. Numerical and experimental responses and the stress-strain diagram are in very good agreement.

4. Response of all Structures

4.1 Failure Modes of Masonry arc Structures

The FE method was used to support the simulation of masonry structures. Figure (6) shows the first and second frequencies and the mode of the structures.

In all structures, the first and second failure modes occurred in the rib cover (Figure 6). In structure 1 with one or two spans, the higher failure modes observed in the rib cover and the bases. However, in three-span structure 1, deformation in the middle span was much less than in the two side spans in the fourth mode. In two-span structure 2,

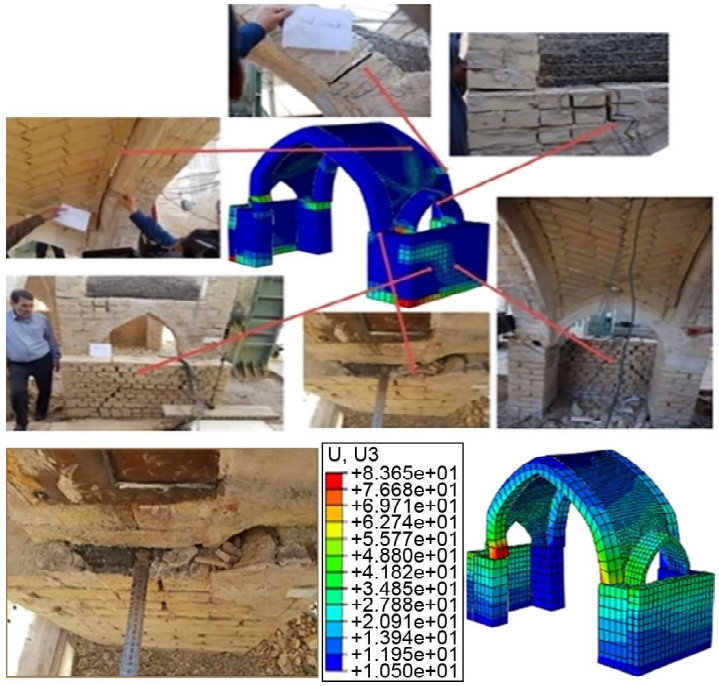

(a) Experimental Tests

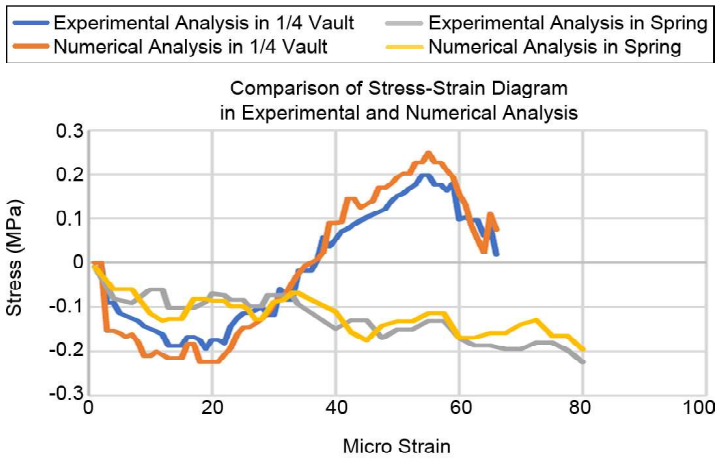

(b) Stress – Strain Diagram

Figure 5. Comparison of numerical analysis and experimental tests (Taghi Panahi et al., 2023).

	1-Span Mode I	1-Span Mode II	2-Span Mode I	2-Span Mode II	3-Span Mode I	3-Span Mode II
Structure1	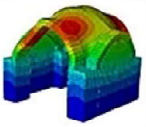	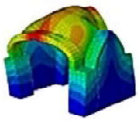	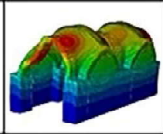	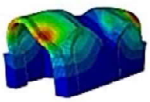	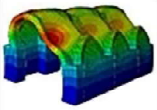	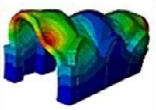
Frequency (Hz)	7.876	12.354	8.165	12.806	8.2624	13.198
Structure1	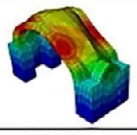	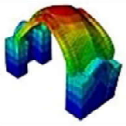	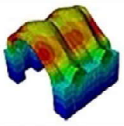	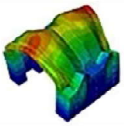	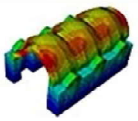	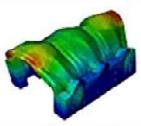
Frequency (Hz)	7.605	8.091	7.8195	10.508	7.897	11.455
Structure1	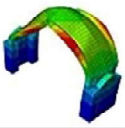	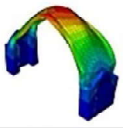		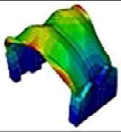	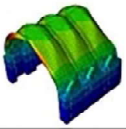	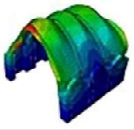
Frequency (Hz)	6.64	6.654	6.978	8.8812	7.0993	10.095

Figure 6. Deformed shapes of structures in the first and second natural modes and frequencies.

the infilling wall between the columns had in-plane movement. However, in two-span structure 2, the movement of the filling wall was out-of-plane. In three-span structure 2, the filling wall of the middle span did not move in the fourth mode. However, in the fifth mode, all the filling walls exhibited in-plane movement.

4.2. Response of Structure 1 to Near-Fault and Far-Fault Ground Motions

Structure 1 has thick vaults and springs placed on strong and large foundations. This structure investigated with three different heights of 5, 6 and 7 m, and the following results obtained. The square plan can be one of its features. The maximum displacement in multi-span structures for the E3 record obtained in the spring direction.

However, for the Coyote Lake far-fault record, the displacement was more significant for the near-fault record. For all structures with different heights and in the direction of the spring, the displacement decreases with the increasing number of the second span. The percentage of reduction in displacement in Third span was about 5-8% more than second span. In the direction of the vault, in a structure with a height of 5 m, the effect of the third span reduces the displacement of the structure up to twice that of the second span. In the structure with a height of 6-7 m, a 4-6% reduction in displacement has observed.

In the direction of loading in the vault and the spring, the ratio of the vault/spring in the structure with various heights is different. In the structure with a height of 5 m, increasing the second span, a very small decrease rate has observed, and in the third span, this rate remains approximately constant. But in structures with a height of 6 and 7 m, a decrease in displacement was observed at a constant rate with the increase of spans from 1 to 3. In the direction of loading in the spring at all heights, the displacement reduction rate is minimal and has a constant slope. This ratio ranges from 35 to 40%. Figure (7).

In the direction of loading in the vault, the displacement increase ratio in the structures with a height of 5 and 6 m, and the 2 and 3 spans are very close to each other, which increases with a minimal slope and at a constant rate. In the direction of the spring, this slope is slightly higher than the direction of the vault, which has increased by about 2-4% in different accelerations. The displacement at the height of 6 and 7 m in the direction of loading in the vault has decreased with the increasing number of spans, and the slope reduction ratio is about 3-6%. In the direction of the spring, this ratio varies in different accelerations, and in the third span, the displacement decreases with a smaller slope. These show that the third span in the structure with a high height had a more significant impact.

The place of maximum displacement in the structures with different heights is variable. In the

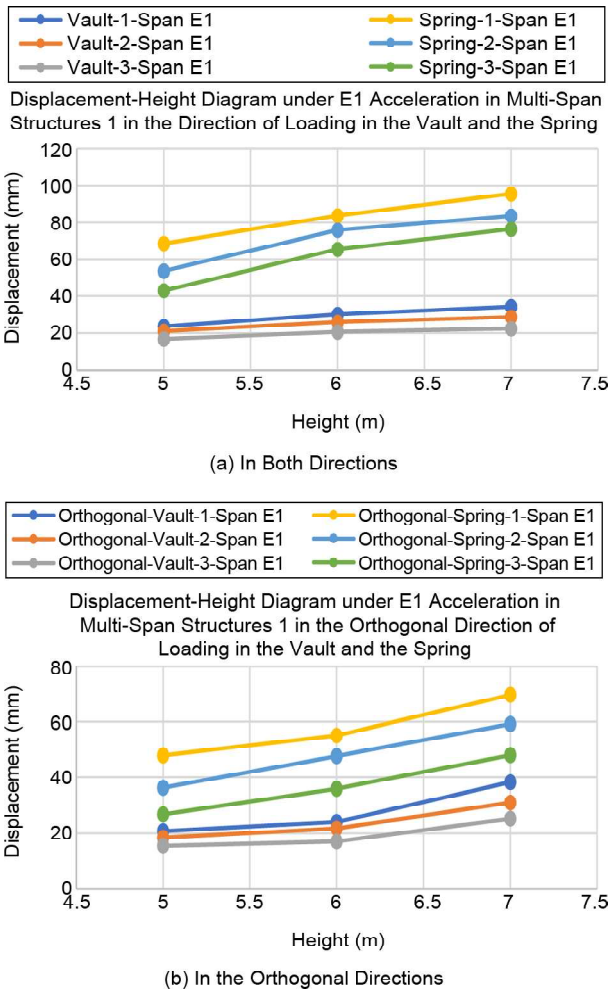

Figure 7. Vault/spring ratio of displacement in multi-span structure 1 and all heights under near-fault acceleration (Coyote Lake).

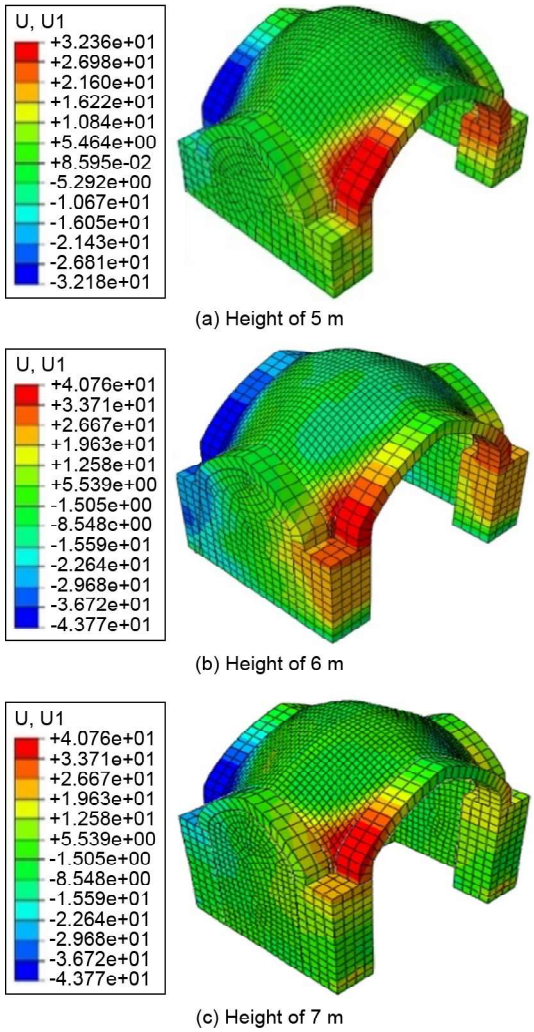

Figure 8. Displacement in one-span Structure 1 at different heights in the direction of the vault under near-fault acceleration (Westmorland).

one-span structure with a height of 5 m, in the direction of the vault, the most displacement is created in the middle of the vault to the top and the bottom, which is the place of the hinges. In the high-frequency content accelerations, maximum displacement has continued towards the top of the structure, which causes the hinges and large displacements have observed. By increasing the number of spans to two, when the acceleration enters the structure, the maximum displacement occurs at the bottom of the structure. When the acceleration exits the structure, the maximum displacement occurs in the vault and roof, which to be appeared the bending failures. By reducing the frequency content and the far-field acceleration, the maximum displacement has created on one side of the structure at the top and on the other side at the bottom towards the bases. In the three-span structure, the middle span has no maximum displacement. In the one-span structure, with the increasing height, the maximum displacement is stretched to 1.4 vault to base, which causes significant moments to be created at the connection point of the roof to the bases, and the maximum displacements occur in these areas Figure (8).

Under the high-frequency-content accelerations, a significant plastic strain occurs in the structure, which starts from the connection of the vault and the spring to the roof and expands to the roof. The structure with a height of 7 meters has had out-of-plane movements at the bases, which is associated with high tensile strains and causes shear-sliding failures. The place of connection of the vault and the spring to the roof is longitudinal fractures along with the crushing of the masonry elements, which can lead to the separation of the ceiling. In low-frequency-content accelerations, the value of plastic strains is less than the maximum plastic strain under pressure Figure (9).

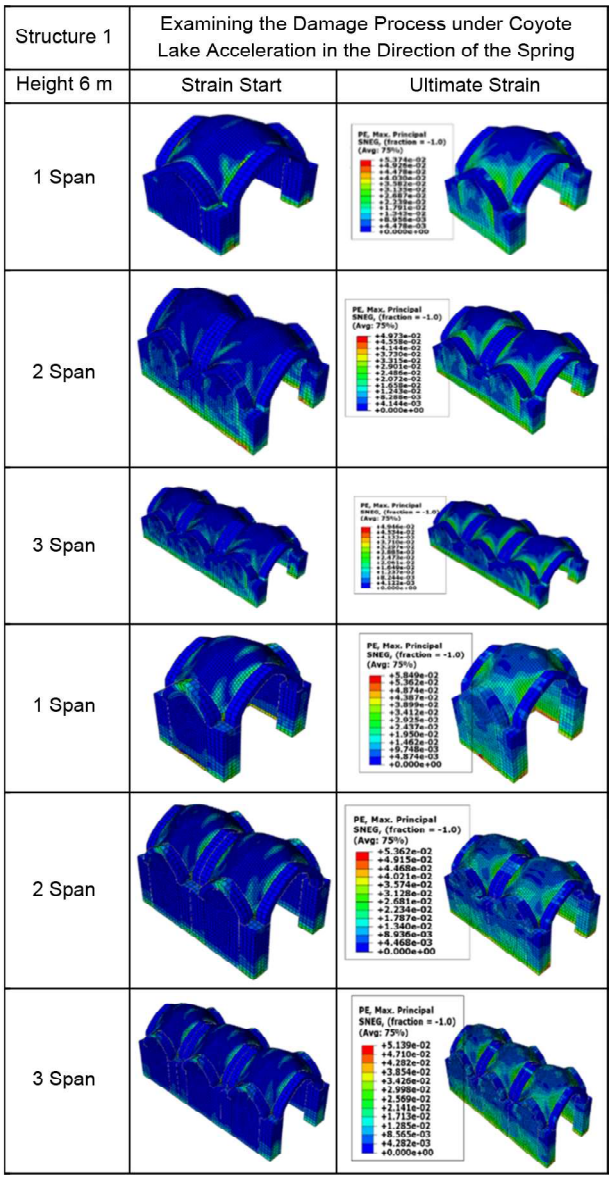

Figure 9. Plastic strain in structure 1 under near-fault and far-fault Coyote Lake acceleration.

4.3. Response of Structure 2 to Near-Fault and Far-Fault Ground Motions

Structure 2 featured a rectangular plan with medium-thickness vaults and springs. It has been investigated at three heights of 3.85, 4.85 and 5.85 meters. The structure experienced six distinct accelerations from two directions. The multi-span structures showed the most significant displacement under the near-fault E3 record. Under the E2 record, notable displacement occurred in the direction of the spring. Increasing the number of spans resulted in reduced displacement. In the analysis of the vault's loading and the displacement of the structure with one to two spans and two to three spans, it was observed that the displacement at heights of 5 and 6 m decreased by approximately 20-30% from one to two spans. The third span has decreased with a lower slope rate. In the structure with a height of 7 m, this decreasing process has become much less with the increase in the number of spans, so that in the two-span structure, it has become half of the other two structures, and in the three-span structure, there was an increase of 5-10%. The displacement ratio of the vault to the spring in the direction of loading in the vault and the spring with the increasing the second span, the reduction ratio has done slowly. In the third span, this decreasing process has increased to 3-5%. In the orthogonal directions of loading, as the number of spans increases, the rate of reduction in structures with heights of 5 and 6 m is greater than that in a structure with a height of 7 m. The number of spans in these two structures significantly impacts the reduction of displacement, with ratios ranging from 50% to 65% (Figure 10).

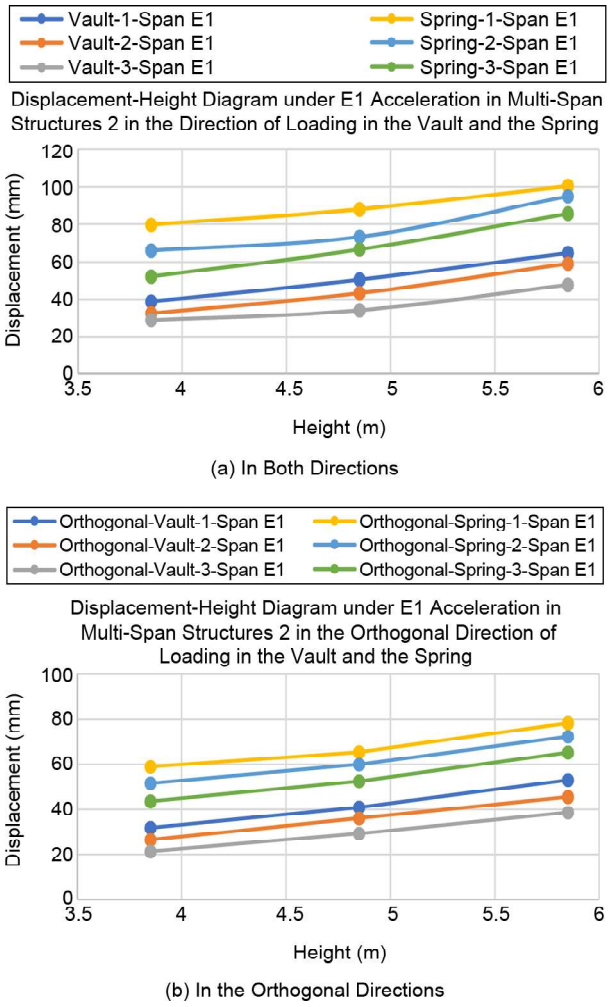

Figure 10. Vault/spring ratio of displacement in multi-span structure 2 and all heights under near-fault acceleration (Coyote Lake).

With the increase in height, displacement has increased, which is normal. In the direction of loading in the vault and the spring, this value varies in different accelerations and at a height of 5 to 6 m. In the second and third spans in the direction of the vault, the decrease was more by 1-2%. In the direction of loading in the spring, in different accelerations, the decreasing process of displacement has been variable and sometimes constant, but generally, this process is upward. Regarding the height of 6 to 7 m, the growth rate was the same in both directions of the structure. The percentage of reduction in displacement in the far-fault accelerations is more than the near-fault, Therefore, the displacement reduction is about 25% in the near-fault accelerations and 30-50% in the far-fault accelerations.

The maximum displacement in the direction of the spring occurred during loading on both sides of the structure, and hinge and fracture observed in these areas in all structures. It can say that the spring performance was very poor. When the acceleration is applied to the structure in the direction of the vault, the high-frequency-content accelerations and the one-span structure, the maximum displacement is created at the top of the structure, but the bases also had a large displacement. But in other accelerations, the maximum displacement appears in 1.4 vaults towards the bases. The hinge created in this area, and displacement also appears at the connection of the base to the rib cover. But in other accelerations, the maximum displacement appears only in 1/4 vaults towards the bases. By increasing the number of spans, the area of the maximum displacement in the first span is at the top and in the end span is at 1.4 vaults. By increasing at the height, maximum displacements do not appear at the top of the structure. In the three-span structure, the middle span does not have a large displacement, and only the spans on both sides of the structure at the top and 1.4 vaults have had maximum displacement, and hinge has appeared in those areas (Figure 11).

The amount of plastic strain is higher than the compressive strains defined for the structure. The strains were observed at the connection of the spring to the roof, which is the beginning of the damage in the structure (Figure 12).

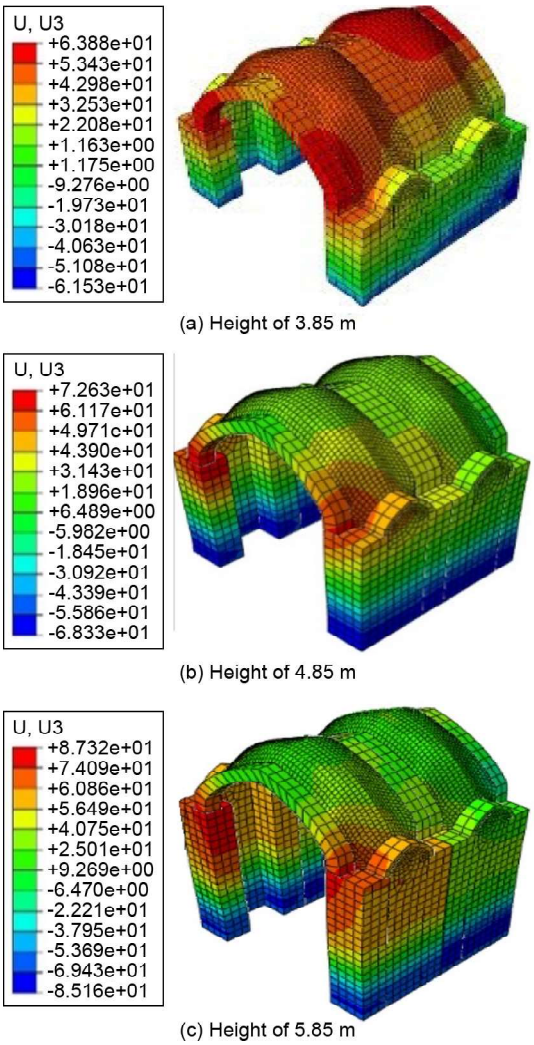

Figure 11. Displacement in one-span structure 1 at different heights in the direction of the vault under near-fault acceleration (Westmorland).

4.4. Response of Structure 3 to Six Near-Fult and Far-Fault Ground Motions

Structure 3 had a rectangular plan with a very long side. The narrow vaults and the springs located on a thin foundation. The structure has investigated with heights of 4.2, 5.2 and 6.2 m. Increasing the number of spans, a decrease in displacement has seen, which shows that the number of spans can have a positive effect in reducing the displacement process in structures. The impact of the third span is very variable compared to the second span. In such a way, in near-fault and high-frequency-content accelerations, the third span had less effect in this decreasing process. In far-fault and lower-frequency-content accelerations, the third span had a more significant impact, which varies by 10-25%. In the

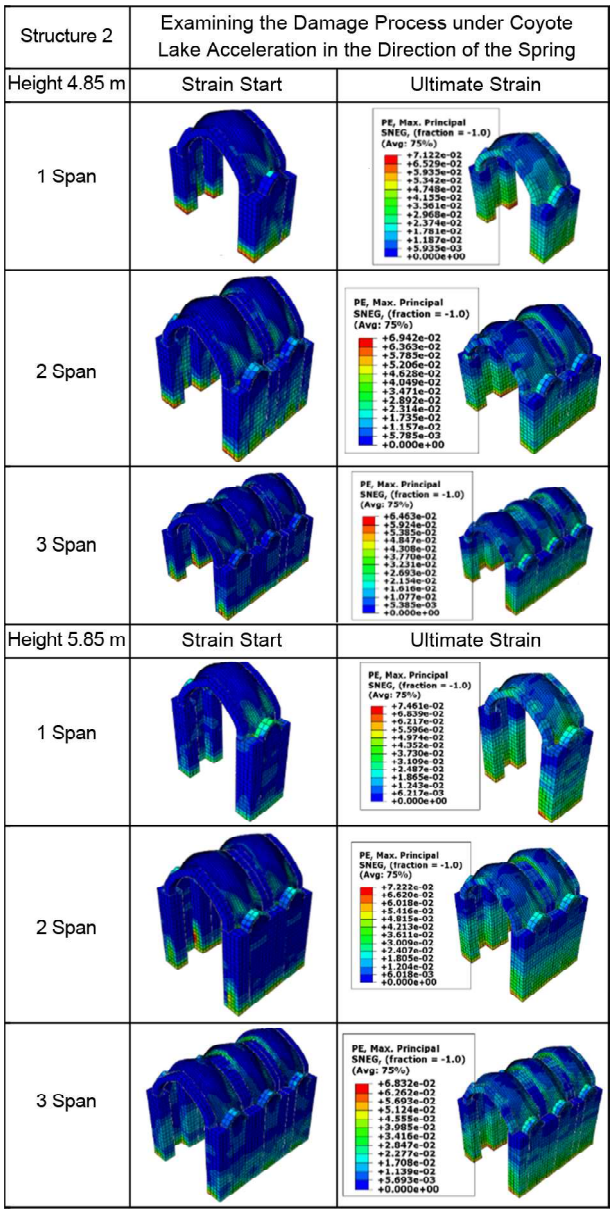

Figure 12. Plastic strain in structure 2 under near-fault and far-fault Coyote Lake acceleration.

direction of the vault, increasing the spans in all accelerations has reduced displacement by 10 to 20%.

The ratio of the displacement of the vault to the spring is minimal in the direction of loading and its orthogonality, which varies from 18 to 23%, and shows that the displacement in the direction of the vault was much less than that of the spring. One of the reasons for these low displacements in the vault is massive displacements in the direction of the spring, which quickly destroys the structure and does not allow the structure to move much in the direction of the vault. Although the displacement has decreased with increasing the number of spans, due to its slight slope, it could not have a good

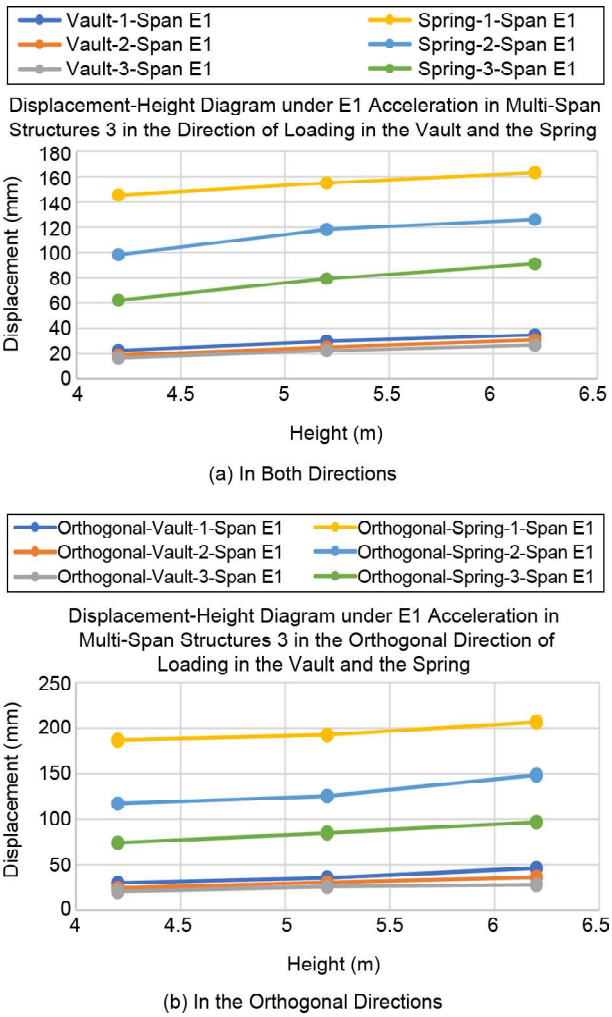

Figure 13. Vault/spring ratio of displacement in multi-span structure 1 and all heights under near-fault acceleration (Coyote Lake).

effect on the structures. So, 1-2% reduction in displacement has observed, which is very insignificant (Figure 13).

Increasing the height of these structures from 4.2 to 5.2 m has increased the displacement in the direction of the vault. The increasing process is very evident in low-frequency-content accelerations. The structure has performed more reasonably under these accelerations. Increasing the height from 5.2 to 6.2 m, the structure's performance in high-frequency-content accelerations and high duration has been so weak that the structure is quickly destroyed and does not allow the structure to move more. In low-frequency-content accelerations and the direction of loading, the displacement has increased by about 30 to 40%.

The maximum displacement in the structure with a height of 4.2 m occurred at 1/4 vault to bottom. However, in the high-frequency-content

accelerations, the bottom of the structure also had large displacements. By increasing the height, the maximum displacements are observed at the top of the structures, which indicated the hinge is created above the structure. Of course, the out-of-plane movements of the filling walls can see with sliding-shearing fractures, which have reached their maximum value in the structure with a height of 6.2 m. Massive out-of-plane movements can see in the bases in all structures, which become much more with increasing height. Of course, bending fractures in the roof can see in all structures. Height can cause severe damage to the structure, but the displacement location has not changed. In some structures, the place of maximum displacement expanded towards connection the vault to the base. By increasing the number of spans, the maximum displacement observed at the connection of the vault to the base, which shows that bending fractures have also involved the base. In two-span structures, both spans have maximum displacement at the top of the vault or the roof and the connection of the vault to the bases, this value reduced with the third span, and the middle span has less displacement than the side spans. The out-of-plan movements of the bases have improved (Figure 14).

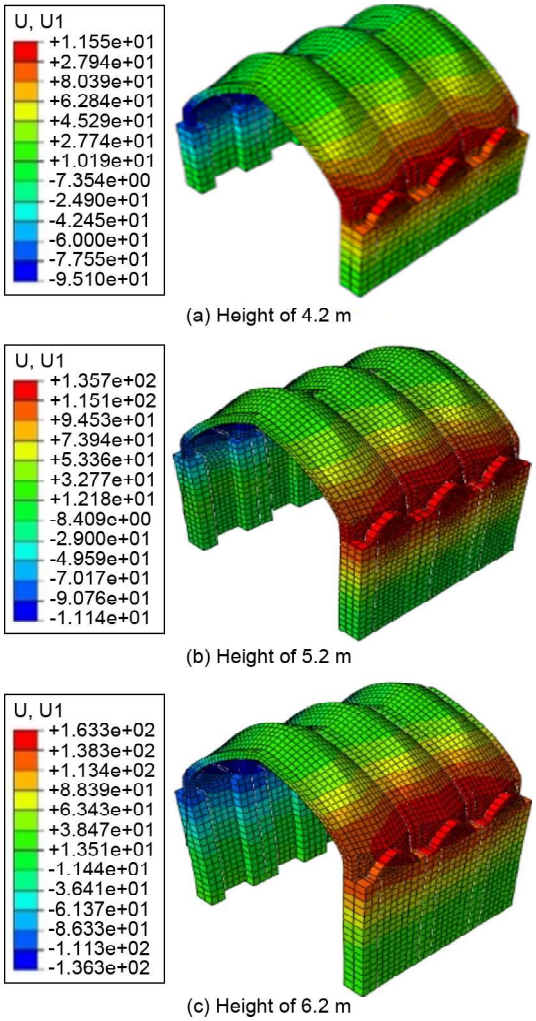

Figure 14. Displacement in one-span Structure 3 at different heights in the direction of the spring under near-fault acceleration (Westmorland).

The plastic strain has been so high that the structure destroyed under tensile and pressure strains, which are the main factors in damage. Bases damaged by large out-of-plane movements. Compressive strains also destroy the structure by crushing the elements, which can see at the connection of the spring to the roof. The process of damage starts from the connection of the vault to the roof and continues to the top of the roof. Of course, the bases have also had great strains. One of the essential features of the rectangular plan is the separation of the filler wall from the side bases (Figure 15).

4.5. Effects on Nine Structures of Six Near-Fault and Far-Fault Ground Motions

The frequency content and parameters such as the amplitude and duration are essential characteristics of an earthquake record that can use to estimate the damage to a structure. The results showed that the linear and non-linear responses of the structures were significantly affected by the frequency content of the accelerations. The frequency content has a significant effect on the response of the structure; thus, it analyzed in both the narrow and broadband ranges. The narrow band covers a small frequency range and most of the far-fault acceleration fell into this category. The broadband frequencies fell into an extensive range, and most near-field accelerations were in this category. E3 acceleration has a lower seismic acceleration peak than E1, but it caused severe damage to all structures. The reason for this was its high-frequency content. In the primary frequency range, this peak acceleration was powerful. Also, its duration was 8 s, which was longer than the duration of E1, which caused a significant change in the structure.

It determined from the seismic response studies of the structures that the parameter that caused an

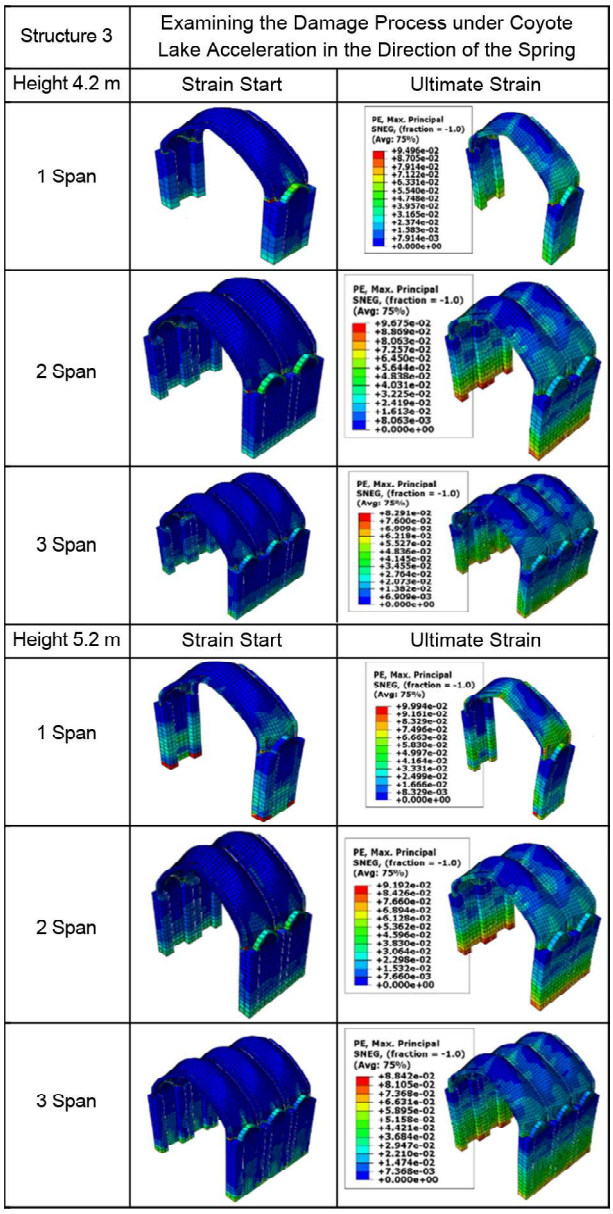

Figure 15. Plastic strain in Structure 3 under near-fault and far-fault Coyote Lake acceleration.

increase in structural damage was the frequency content of the earthquake (Afreen et al., 2021). By comparing three structures with different spans, it can see that structure 1 had less displacement than the other two structures at all heights, which shows that it performed much better. The maximum displacement in three structures was at 1.4 vaults, which was almost the same in all structures, and by increasing the height, the location of the maximum displacement changes.

The out-of-plane movements of the bases with the separation of the filling wall in the high structure with a rectangular plan can be seen well. Slip-shear fractures in bases can see especially in high-frequency-content accelerations. The process of reducing the displacement in the valve/spring ratio of displacement in structure 1 is more than in the other two structures, which shows that the two directions of the structure have displaced close to each other. But in the structure with a rectangular plan, the direction of the spring has had much larger displacements than the direction of the vault.

5. Conclusion

- Multi-span structures with different heights, and having different dimensions in plan investigated. Six near-fault and far-fault accelerations selected with different durations, distances to the fault and ground accelerations. These records applied to the structures separately in the directions of the vault and the spring. The following results obtained:
- When the plan is closer from the square to the rectangle, the structure's performance weaker and the stiffness and resistance reduced. Also, with increasing height, this weakness is more evident. The increase in displacement from structure 1 to 2 in three heights of about 12, 18 and 20% and from structure 2 to 3 in three heights of 57, 70 and 75% has reported. Therefore, the narrower the structure becomes, the faster its stiffness decreases.
- In all plans, with the decrease in the height of the bases, sliding-shear behavior is seen, and with the increase in the height of the base, the out-of-plane movements cause flexural failure due to the slenderness and increase of the anchor.
- In a structure with a rectangular plan, pressure damage spreads from the top of the spring to the middle of the roof and the connection point of the spring to the roof, as well as the side parts. If in the square plan, most of the damage is from the connection point of the spring to the vault. In the rectangular plan, high tensile strains and damage caused by it are more evident.
- In all three types of geometry and plan, increasing the height of the structure has a significant effect on increasing displacement. But since the roof system is also very essential, which saw in the first mode of vibration, this height in crease effect is not significant. But with the increase in height, the slope of the increase in

displacement in the structure 1 becomes slower. But in the second structure, which is narrower, the growth rate of deformation at higher heights is faster. Due to the rectangular plan, the effect of height on the performance of the structure is more evident, in such a way that in increasing the base height to 2.8 m, about 10% and in height to 3.8 m, about 20% increase in displacement observed. The growth rate of displacement with increasing height is higher in the direction of the spring than in the direction of the vault. In the narrower structure, with the increase in height, the difference in the displacement of the spring to the vault has increased significantly and has been reported up to five times.

- The process of damage in the structure with a square plan starts from the connection of the vault and the spring to the roof, and in the structure with a rectangular plan, this process starts from the connection of the spring to the roof and spreads throughout the structure.
- In the structure with $L/B=3.3$ and the rectangular plan, the foundation exhibited out-of-plane movement, and the structures sustained damage. Although the displacement decreased strongly in the three-span structure, out-of-plane movement observed. In some structures, the most significant displacement occurred in the foundations or at the bottom of the structure (Bayraktar & Hökelekli, 2020; Llopis-Pulido et al., 2019).

References

Abdulla, K. F., Cunningham, L. S., & Gillie, M. (2017). Simulating masonry wall behaviour using a simplified micro-model approach. *Engineering Structures*, *151*, 349-365. doi: 10.1016/j.engstruct.2017.08.021

Afreen, A., Ahmed, A., & Moin, K. (2021). Effect of near-field earthquake on masonry structure. *Asian Journal of Civil Engineering*, 0123456789. doi: 10.1007/s42107-021-00353-4

Altunis Sik, A. C., & Genç, A. F. (2017). Earthquake response of heavily damaged historical masonry mosques after restoration. N*atural Hazards and Earth System Sciences*, *17*(10), 1811-1821. doi: 10.5194/nhess-17-1811-2017

Atmaca, B., Demir, S., Günaydin, M., Altunisik, A. C., Hüsem, M., Ates, S., Adanur, S., & Angin, Z. (2020). Field Investigation on the Performance of Mosques and Minarets during the Elazig-Sivrice Earthquake. *Journal of Performance of Constructed Facilities*, *34*(6). doi: 10.1061/(asce)cf.1943-5509.0001527

Bartoli, G., & Betti, M. (2013). Cappella dei principi in firenze, Italy: experimental analyses and numerical modeling for the investigation of a local failure. *Journal of Performance of Constructed Facilities*, *27*(1), 4-26. doi: 10.1061/(asce)cf.1943-5509.0000315

Bayraktar, A., & Hökelekli, E. (2020). Seismic performances of different spandrel wall strengthening techniques in masonry arch bridges. *International Journal of Architectural Heritage*, 00(00), 1-19. doi: 10.1080/15583058.2020.1719234

Bertolesi, E., Milani, G., Carozzi, F. G., & Poggi, C. (2018). Ancient masonry arches and vaults strengthened with TRM, SRG and FRP composites: Numerical analyses. *Composite Structures*, *187*, 385-402. doi: 10.1016/j.compstruct.2017.12.021

Cao, V. Van, & Ronagh, H. R. (2014). Correlation between seismic parameters of far-fault motions and damage indices of low-rise reinforced concrete frames. *Soil Dynamics and Earthquake Engineering*, *66*, 102-112. doi: 10.1016/j.soildyn.2014.06.020

Castellazzi, G., D'Altri, A. M., de Miranda, S., Chiozzi, A., & Tralli, A. (2018). Numerical insights on the seismic behavior of a nonisolated historical masonry tower. *Bulletin of Earthquake Engineering*, *16*(2), 933-961. doi: 10.1007/s10518-017-0231-6

Castori, G., Borri, A., De Maria, A., Corradi, M., & Sisti, R. (2017). Seismic vulnerability assessment of a monumental masonry building. *Engineering Structures*, *136*, 454-465. doi: 10.1016/j.engstruct.2017.01.035

D'Altri, A. M., Messali, F., Rots, J., Castellazzi, G., & de Miranda, S. (2019). A damaging block-based model for the analysis of the cyclic behaviour of full-scale masonry structures. *Engineering Fracture Mechanics*, 209(July), 423-448. doi: 10.1016/j.engfracmech.2018.11.046

Davoodi, M., Jafari, M. K., & Hadiani, N. (2013). "Seismic response of embankment dams under near-fault and far-field ground motion excitation. *Engineering Geology*, *158*, 66-76. doi: 10.1016/j.enggeo.2013.02.008

Federal Emergency Management Agency. (2009). *Quantification of Building Seismic Performance Factors* (FEMA P-695).

Gönen, S., & Soyöz, S. (2021). Seismic analysis of a masonry arch bridge using multiple methodologies. *Engineering Structures*, *226*(September 2020). doi: 10.1016/j.engstruct.2020.111354

Grimaz, S., & Malisan, P. (2014). Near field domain effects and their consideration in the international and Italian seismic codes. *Bollettino Di Geofisica Teorica Ed Applicata*, *55*(4), 717-738. doi: 10.4430/bgta0130

Güllü, H., & Karabekmez, M. (2017). Effect of near-fault and far-fault earthquakes on a historical masonry mosque through 3D dynamic soil-structure interaction. *Engineering Structures*, *152*, 465-492. doi: 10.1016/j.engstruct.2017.09.031

Gunes, B., Cosgun, T., Sayin, B., Ceylan, O., Mangir, A., & Gumusdag, G. (2021). Seismic assessment of a reconstructed historic masonry structure: A case study on the ruins of Bigali castle mosque built in the early 1800s. *Journal of Building Engineering*, 39(February), *102240*. doi: 10.1016/j.jobe.2021.102240

Hatzigeorgiou, G. D. (2010). Behavior factors for nonlinear structures subjected to multiple near-fault earthquakes. *Computers and Structures*, *88*(5-6), 309-321. doi: 10.1016/j.compstruc.2009.11.006

Hemeda, S. (2019). 3D finite element coupled analysis model for geotechnical and complex structural problems of historic masonry structures: conservation of Abu Serga church, Cairo, Egypt. *Heritage Science*, *7*(1), 1-19. doi: 10.1186/s40494-019-0248-z

Khan, W., Akhtar, S., & Hussain, A. (2019). Rehabilitation of concrete and masonry structures. *AIP Conference Proceedings*, 2158(September). doi: 10.1063/1.5127152

Kujawa, M., Lubowiecka, I., & Szymczak, C. (2020). Finite element modelling of a historic church structure in the context of a masonry damage analysis. *Engineering Failure Analysis*, *107*, 104233. doi: 10.1016/j.engfailanal.2019.104233

Llopis-Pulido, V., Durá, A. A., Fenollosa, E., & Martínez, A. (2019). Analysis of the structural behavior of the historical constructions: seismic evaluation of the cathedral of valencia (Spain). *International Journal of Architectural Heritage*, *13*(1), 205-214. doi: 10.1080/15583058.2018.1497221

Masciotta, M. G., Ramos, L. F., Lourenço, P. B., & Vasta, M. (2017). Damage identification and seismic vulnerability assessment of a historic masonry chimney. *Annals of Geophysics*, *60*(4). doi: 10.4401/ag-7126

Micelli, F., & Cascardi, A. (2020). Structural assessment and seismic analysis of a 14th century masonry tower. *Engineering Failure Analysis*, *107*(October), 104198. doi: 10.1016/j.engfailanal.2019.104198

Milani, G., & Lourenço, P. B. (2012). 3D non-linear behavior of masonry arch bridges. *Computers and Structures*, *110-111*, 133-150. doi: 10.1016/j.compstruc.2012.07.008

Milani, G., & Valente, M. (2015). Failure analysis of seven masonry churches severely damaged during the 2012 Emilia-Romagna (Italy) earthquake: Non-linear dynamic analyses vs conventional static approaches. *Engineering Failure Analysis*, *54*(May 2012), 13-56. doi: 10.1016/j.engfailanal.2015.03.016

Nasiri, E., & Liu, Y. (2017). Development of a detailed 3D FE model for analysis of the in-plane behaviour of masonry infilled concrete frames. *Engineering Structures, 143*, 15 July 2017, Pages 603-616. doi: 10.1016/j.engstruct.2017.04.049

Özmen, A., & Sayin, E. (2018). Seismic assessment of a historical masonry arch bridge. *Journal of Structural Engineering & Applied Mechanics*, *1*(2), 95-104. doi: 10.31462/jseam.2018.01095104

Özmen, A., & Sayin, E. (2021). Seismic response of a historical masonry bridge under near and far-fault ground motions. *Periodica Polytechnica Civil*

Engineering, *65*(3), 946-958. doi: 10.3311/PPci.17832

Seker, B. S., Cakir, F., Dogangun, A., & Uysal, H. (2014). Investigation of the structural performance of a masonry domed mosque by experimental tests and numerical analysis. *Earthquake and Structures*, *6*(4), 335-350. doi: 10.12989/eas.2014.6.4.335

Stockdale, G., Tiberti, S., Camilletti, D., Sferrazza Papa, G., Basshofi Habieb, A., Bertolesi, E., Milani, G., & Casolo, S. (2018). Kinematic collapse load calculator: Circular arches. *SoftwareX*, *7*, 174-179. doi: 10.1016/j.softx.2018.05.006

Szolomicki, J., Berkowski, P., & Baranski, J. (2015). Computer modelling of masonry cross vaults strengthened with fiber reinforced polymer strips. *Archives of Civil and Mechanical Engineering*, *15*(3), 751-766. doi: 10.1016/j.acme.2014.05.006

Taghi Panahi, F., & Akbarzadeh Morshedi, A. A. (2020). Experimental investigation of brick masonry arches' (Vault and Rib cover) behavior unreinforced and reinforced by C-FRP under vertical and horizontal Load simultaneously. *Advance Researches in Civil Engineering*. ISSN: 2645-7229, *2*(3), 41-50.

Taghi Panahi, F., Akbarzadeh Morshedi, A. A, & Talaeitaba, S. B. (2023). Effects of the structural dimensions of multi-span historical arched masonry buildings under near-fault and far-fault ground motions. *Engineering Failure Analysis*. doi: 10.1016/j.engfailanal.2023.107685

Taghi Panahi, F., & Akbarzadeh Morshedi, A. A. (2024). The effect of geometry (height and plan) on seismic response of historical multi-span masonry arch structures. 9th *International Conference on Seismology and Earthquake Engineering (SEE9-04920419)*. Tehran, Iran.

Talebi Jouneghani, K., Hosseini, M., Rohanimanesh, M. S., & Raissi Dehkordi, M. (2017). Evaluating main parameters effects of near-dield warthquakes on the behavior of concrete structures with moment frame system. A*dvances in Science and Technology Research Journal*, *11*(3), 10-23. doi: 10.12913/22998624/74135

Tiberti, S., Acito, M., & Milani, G. (2016). Comprehensive FE numerical insight into Finale Emilia Castle behavior under 2012 Emilia Romagna seismic sequence: Damage causes and seismic vulnerability mitigation hypothesis. *Engineering Structures*, *117*, 397-421. doi: 10.1016/j.engstruct.2016.02.048

Valente, M., & Milani, G. (2019). Damage assessment and collapse investigation of three historical masonry palaces under seismic actions. *Engineering Failure Analysis*, *98*(January), 10-37. doi: 10.1016/j.engfailanal.2019.01.066

Zampieri, P., Simoncello, N., & Pellegrino, C. (2019). Seismic capacity of masonry arches with irregular abutments and arch thickness. *Construction and Building Materials*, *201*, 786-806. doi: 10.1016/j.conbuildmat.2018.12.063

Zampieri, P., Zanini, M. A., & Faleschini, F. (2016). Influence of damage on the seismic failure analysis of masonry arches. *Construction and Building Materials*, *119*, 343-355. doi: 10.1016/j.conbuildmat.2016.05.024

Zampieri, P., Zanini, M. A., & Modena, C. (2015). Simplified seismic assessment of multi-span masonry arch bridges. *Bulletin of Earthquake Engineering*, *13*(9), 2629-2646. doi: 10.1007/s10518-015-9733-2

Zhao, Ch., Lei, M., Jia, Ch., Yang, Z., & Shi, Y. (2023). An elastoplastic damage model for concrete considering the influence of mesostructure on transverse deformation. *Construction and Building Materials*, September, 1-14. doi: 10.1016/j.conbuildmat.2023.133458